Developmental Biology 454 (2019) 15–20

Contents lists available at ScienceDirect

Developmental Biology

journal homepage: www.elsevier.com/locate/developmentalbiology

Fndc-1 contributes to paternal mitochondria elimination in *C. elegans*

Yunki Lim [a], Karinna Rubio-Peña [b], Peter J. Sobraske [a], Paola A. Molina [c], Paul S. Brookes [d,e], Vincent Galy [b,**], Keith Nehrke [a,e,*]

[a] Department of Medicine, Nephrology Division, School of Medicine and Dentistry, University of Rochester Medical Center, Rochester, NY, 14642, USA
[b] Developmental Biology Laboratory, Sorbonne Université, CNRS, Institut de Biologie Paris Seine, IBPS, UMR7622, Paris, France
[c] Department of Biology, Middle Tennessee State University, 1301 E. Main Street, Murfreesboro, TN, 37132, USA
[d] Department of Anesthesiology, School of Medicine and Dentistry, University of Rochester Medical Center, Rochester, NY, 14642, USA
[e] Department of Pharmacology and Physiology, School of Medicine and Dentistry, University of Rochester Medical Center, Rochester, NY, 14642, USA

ARTICLE INFO

Keywords:
Autophagy
Mitochondria
Mitophagy
Maternal inheritance
C. elegans

ABSTRACT

Paternal mitochondria are eliminated following fertilization by selective autophagy, but the mechanisms that restrict this process to sperm-derived organelles are not well understood. FUNDC1 (FUN14 domain containing 1) is a mammalian mitophagy receptor expressed on the mitochondrial outer membrane that contributes to mitochondrial quality control following hypoxic stress. Like FUNDC1, the *C. elegans* ortholog FNDC-1 is widely expressed in somatic tissues and mediates hypoxic mitophagy. Here, we report that FNDC-1 is strongly expressed in sperm but not oocytes and contributes to paternal mitochondria elimination. Paternal mitochondrial DNA is normally undetectable in wildtype larva, but can be detected in the cross-progeny of *fndc-1* mutant males. Moreover, loss of *fndc-1* retards the rate of paternal mitochondria degradation, but not that of membranous organelles, a nematode specific membrane compartment whose fusion is required for sperm motility. This is the first example of a ubiquitin-independent mitophagy receptor playing a role in the selective degradation of sperm mitochondria.

1. Introduction

Maternal mitochondrial inheritance is widely-conserved among metazoans. However, our understanding of the molecular processes that specify paternal mitochondria elimination (PME) is incomplete. Mitophagy is a process in which mitochondria are engulfed by autophagosomes and delivered to lysosomes for destruction. PME was first reported to occur through mitophagy in the genetic model organism *C. elegans* (Sato and Sato, 2011; Zhou et al., 2011; Al Rawi et al., 2011), and mitophagy has recently been shown to underlie PME in mouse embryos (Rojansky et al., 2016). Nevertheless, the signal that initiates selective degradation of paternal mitochondria following fertilization is unknown.

One form of mitophagy is triggered by the loss of mitochondrial membrane potential ($\Delta\Psi$) in a pathway that requires the E3 kinase PINK1 and E3 ubiquitin ligase Parkin (Whitworth and Pallanck, 2017). In somatic cells, these proteins contribute to mitochondria quality control (MQC) through the selective recognition of damaged mitochondria. Indeed, a loss of membrane potential has been reported to occur in mammalian sperm mitochondria within 36 h of fertilization, and PME engages PINK1, Parkin, and other MQC players to facilitate mitochondrial degradation (Rojansky et al., 2016). However, PINK1 mostly functions as a sentinel that recognizes mitochondrial damage and is not causative for mitophagy in-and-of itself. Furthermore, the deletion mutants in the PINK1-Parkin pathway in *C. elegans* are not affected for the degradation of sperm mitochondria nor the nematode specific membranous organelles (MOs) (Sato et al., 2018).

The identification of new molecules that contribute to PME may help to broaden our understanding of underlying mechanisms and signaling pathways that target sperm mitochondria specifically for degradation. For example, *phb-2* (prohibitin 2) was recently demonstrated to form a paternal mitophagy receptor at the mitochondrial inner membrane in *C. elegans* (Wei et al., 2017). It is notable however that outer membrane rupture is necessary to unveil the PHB-2 receptor, making this an unlikely candidate for an initial selectivity filter.

Alternative modes of mitophagy involve mitochondrial outer

* Corresponding author. Department of Medicine, Nephrology Division, Box 675, University of Rochester Medical Center, 601 Elmwood Avenue, Rochester, NY, 14642, USA.
** Corresponding author. UMR7622 CNRS-SU, Biologie du Développement, Box 24, Sorbonne Université 9 quai Saint-Bernard, 75252, Paris, Cédex 05, France.
E-mail addresses: vincent.galy@upmc.fr (V. Galy), keith_nehrke@urmc.rochester.edu (K. Nehrke).

https://doi.org/10.1016/j.ydbio.2019.06.016
Received 12 February 2019; Received in revised form 29 May 2019; Accepted 20 June 2019
Available online 21 June 2019

membrane receptors that can recruit autophagosomes through direct binding to microtubule-associated protein light chain 3 (LC3), including BNIP3, NIX, and FUNDC1 (Yoo and Jung, 2018). This hypothesis is an attractive alternative to other autophagy pathways since paternal mitochondria in *C. elegans* do not seem to be strongly ubiquitinated (Sato et al., 2018; Hajjar et al., 2014). These receptors are thought to operate independent of PINK1 and Parkin in somatic cells. While it is currently unknown whether any of these proteins play a role in PME, which is temporally constrained to a very short period and results in removal of the entire paternal mitochondrial pool, mining of bioinformatics databases suggested that FUNDC1 expression in testes responded to a genetic perturbation expected to impact MQC differently than nearly all somatic tissues (NCBI GEO GDS4791/1424215_PM_at "Mitochondrial protease Clpp knockout effect on various tissues").

FUNDC1 was identified based upon its ability to facilitate clearance of mitochondria damaged by exposure to hypoxia and selectively associates with LC3B (Wu et al., 2016). LC3 binding is regulated by reversible phosphorylation via ULK1 and PGAM5 (Wu et al., 2014a, 2014b). FUNDC1 is localized to the mitochondria outer membrane at sites of contact with ER (Wu et al., 2016), where it interacts with both the IP3 receptor and components of the mitochondrial fission-fusion machinery (Wu et al., 2017a). In mice, FUNDC1 contributes to cardiac health and modulates ischemia-reperfusion injury (Wu et al., 2017a; Zhang et al., 2016).

We recently found that the *C. elegans T06d8.7/fndc-1* gene product, an ortholog to human FUNDC1, is broadly expressed across many somatic tissues where it localizes to the mitochondria and contributes to hypoxic mitophagy (manuscript in preparation). Our results here demonstrate that FNDC-1 is also expressed strongly in the male germ line, where it localizes in sperm mitochondria and acts as a paternal mitophagy receptor that contributes to the uniparental inheritance of mitochondria.

2. Results

2.1. Expression of fndc-1 in C. Elegans sperm mitochondria

The predicted gene *T06D8.7/fndc-1* codes for a protein that shares 32% identity and 50% similarity to human FUNDC1 and is the second gene in a *C. elegans* operon that includes a non-ATPase subunit of the 26S proteasome's 19S regulatory particle base subcomplex *rpn-9*, cytochrome *c*-type heme lyase *cclh-1*, and cytochrome *c* oxidase assembly factor *cox-15*. As might be expected based upon the other genes in this operon, a CRISPR-Cas9 fusion (Paix et al., 2017) between mRuby3 and *fndc*-1 is broadly expressed in many somatic tissues (Fig. 1A), consistent with its expression in mice (Liu et al., 2012). Robust levels of mRuby3 fluorescence were also observed in both the hermaphrodite spermatheca (Fig. 1B) and the male gonad (Fig. 1C). In dissected male gonads, the mRuby3::FNDC-1 fusion protein were found to label the spermatids (Fig. 1D). Likewise, closer examination of the hermaphrodites revealed brightly labeled sperm surrounded by dimmer surrounding somatic tissue, and oocytes which lacked appreciable *fndc-1* expression entirely. Finally, the mRuby3::FNDC-1 fusion protein appeared to co-localize in spermatids with a CRISPR-Cas9 mediated insertion of GFP coding sequencing to *ucr-2.3*, coding for the complex III ubiquinol-cytochrome c reductase core protein 2 of the mitochondrial electron transport chain (Fig. 1E), and localized in mature spermatazoa to the cell body and not to the pseudopod (data not shown), consistent with mitochondrial targeting.

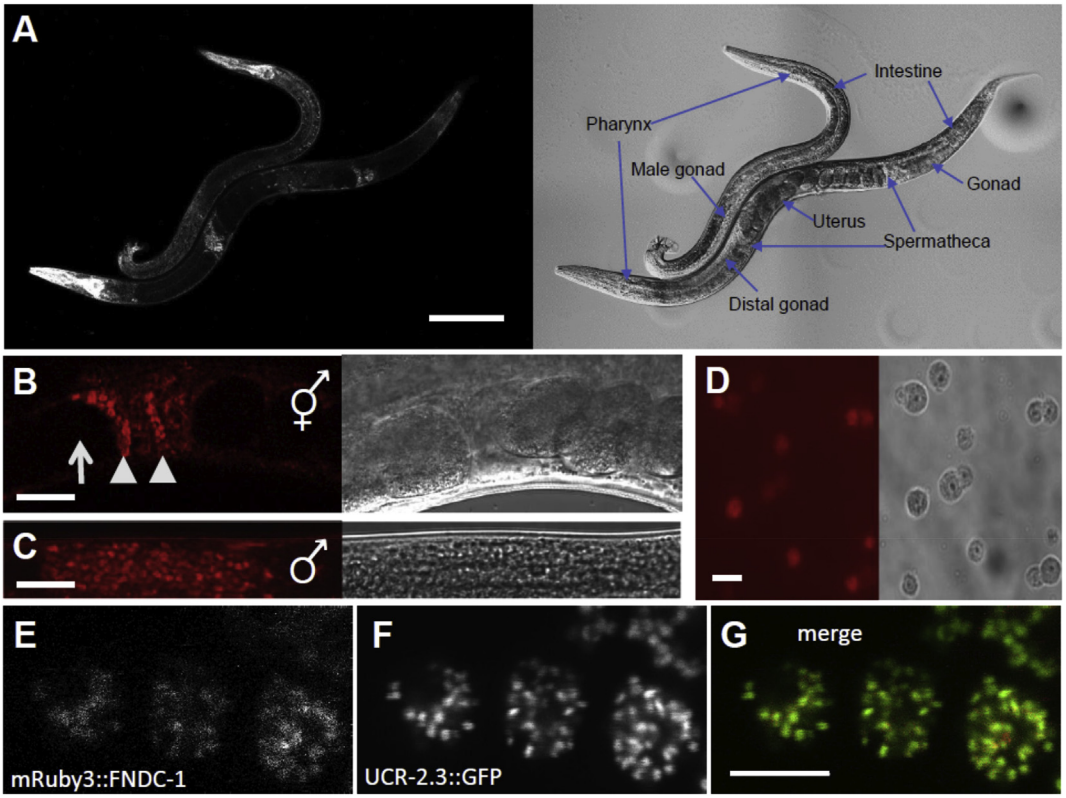

Fig. 1.. FNDC-1 is expressed in spermatids and targeted to mitochondria. mRuby3 red fluorescent protein sequence was inserted into the N-terminal genomic coding region of *fndc-1* using CRISPR-Cas9 editing and HDR. Images in panels A–D contain both fluorescence (left) and differential contrast interference (right). (A) Intestine, body wall muscles, and pharynx of males and hermaphrodites, as labeled. Scale bar: 100 μm. (B) Hermaphrodite spermatheca. Note the lack of expression in oocytes (arrows) compared to spermatids (arrowheads). Scale bar: 20 μm. (C) Male gonad. Scale bar: 20 μm. (D) Isolated spermatids from males expressing mRuby3::FNDC-1. Scale bar: 5 μm. (E) Higher magnification image of mRuby3::FNDC-1 in spermatids. (F) Genomic single copy CRISPR-Cas9 modified *ucr-2.3*:GFP in the same spermatids as panel E. (G) Overlay of mRuby3::FNDC-1 (red) and *ucr-2.3*: GFP (green). Scale bar: 5 μm.

2.2. Paternal mtDNA are detectable in the cross-progeny of fndc-1(lf) males

The differential expression of *fndc-1* in male and female germ cells motivated the question of whether FNDC-1 might also play a role in PME. *uaDf5* is a mitochondrial haplotype represented by a large, stable deletion in the mitochondrial genome (Tsang and Lemire, 2002). Mitochondrial haplotypes are not inherited through Mendelian genetics, but their abundance can be represented through heteroplasmy, which compares the relative amount of mutant to wildtype mitochondrial haplotypes. Within *uaDf5* strains, *uaDf5* generally contributes ~70% of the mitochondrial pool in a non-mutant nuclear genome background (Tsang and Lemire, 2002). Most importantly here, *uaDf5* can be distinguished from wildtype mtDNA via PCR (Gitschlag et al., 2016). When a *uaDf5* male is mated with a *fem-3(e2006)* hermaphrodite that lacks sperm production under non-permissive conditions, it is possible to monitor the removal (or retention) of the male sperm mtDNA by tracking *uaDf5* haplotype by PCR in their progeny.

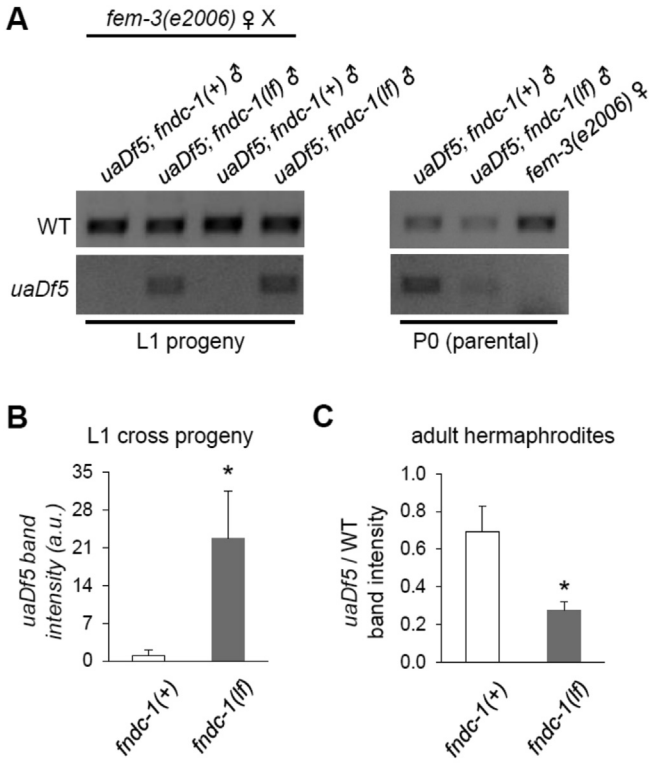

Fig. 2. The paternal mitochondrial genome is detectable in cross progeny of *fndc-1(lf)* males.
The *uaDf5* mitochondrial haplotype is a large deletion in the mitochondrial genome that can be detected by PCR. (A) The first four lanes contain ethidium bromide stained gel-separated PCR products from ~100 L1 cross-progeny of *fem-3(e2006)* females that had been mated to either *fndc-1(+)* or *fndc-1(lf)* males containing *uaDf5* mtDNA. These data are two replicates of six indepenent experiments that were performed. The second set of three lanes are similar PCR reactions from the paternal and maternal worms that were used to create the cross-progeny. Note that amplification cycles (generally 25–35) have been optimized for each of the primer combinations, whether used as pairs or in triplicate, for L1 versus P0 generations, and for multiple versus single worms (see Methods). As such, band intensities are only directly comparable within the boundaries of each image. (B) *uaDf5* in L1 cross-progeny from *fndc-1(+)* or *fndc-1(lf)* males and *fem-3(e2006)* hermaphrodites. The band intensity for the *uaDf5* PCR product was determined and normalized to the wildtype PCR product to control for total mtDNA content. The data represents the average values from six independent experiments (mean ± SEM; *p < 0.05; *t*-test). (C) Relative *uaDf5* abundance in *fndc-1(+)* and *fndc-1(lf)* adult hermaphrodites. The data (for which the PCR reactions are not shown) represents the average values from three independent experiments (mean ± SEM; *p < 0.05; *t*-test).

In the background of a wildtype nuclear genome, residual *uaDf5* mtDNA can be detected by PCR up to but not beyond the 64-cell stage of embryonic development (Zhou et al., 2011). However, previous studies have shown that *uaDf5* mtDNA can be detected in the fully-developed cross-progeny of a *uaDf5* male and an *atg-7(bp422)* autophagy mutant hermaphrodite (Wang et al., 2016); since the worm atg8/LC3 homolog LGGs are necessary to remove paternal mtDNA, this cross results in a similar residual, but detectable level of *uaDf5* in cross-progeny of *uaDf5* males and mutant hermaphrodites (Sato and Sato, 2011; Zhou et al., 2011; Rawi et al., 2011).

Here, either *fndc-1(+); uaDf5* males or *fndc-1(rny14); uaDf5* males were crossed to *fem-3(e2006)* hermaphrodites, and the abundance of the *uaDf5* haplotype was assessed by PCR in recently-hatched L1 cross-progeny. In contrast to *fndc-1(+)* controls, where *uaDf5* mtDNA was minimal, *uaDf5* mtDNA could be amplified from the cross-progeny of *fndc-1(lf)* males (Fig. 2A and B). This result was specific to the male germ line, as maternal *fndc-1(lf)* had no impact on PME following mating by a *fndc-1(+); uaDf5* male (data not shown).

Heteroplasmy is also subject to genetic control, and heteroplasmic tolerance can differ in mutant backgrounds, particularly those that impact MQC. Hence, it was intriguing that the relative abundance of *uaDf5* to wildtype mtDNA was decreased in the paternal *fndc-1(lf)* males (Fig. 2A). A similarly reduced heteroplasmic level was observed in *fndc-1(lf)* hermaphrodites (Fig. 2C). This is akin to the effect reported in other MQC mutants (Lin et al., 2016). However, it is important to note that the decrease in *uaDf5* load in the paternal *fndc-1(lf)* males is likely not responsible for the increased amount of *uaDf5* observed in their progeny. In fact, a reduced amount of *uaDf5* haplotype contributed at fertilization would be expected to reduce, not extend, the time-to-clearance.

2.3. Removal of paternal mitochondria but not membranous organelles is facilitated by fndc-1

Sperm-derived MOs in *C. elegans* function to deliver cargo to the plasma membrane of mature spermatozoon (Shakes and Ward, 1989) and are removed following fertilization through autophagy (Sato and Sato, 2011; Zhou et al., 2011; Rawi et al., 2011). RAB-7 is a small GTPase that regulates membrane traffic into and between early-to-late endosomes and its loss has been shown to delay MO clearance in worms (Djeddi et al., 2015). We also found that depletion of oocyte *rab-7* by RNAi delayed MO clearance in the resulting embryos; however, the absence of FNDC-1 in the sperm did not (Fig. 3). The absence of paternal FNDC-1 did result in a transient and reproducible delay in PME (Fig. 4). In agreement with previous results obtained for mtDNA, this result confirms that paternal *fndc-1* is required for normal sperm mitochondria elimination. This delay being specific to sperm mitochondria degradation reinforces the conclusion made in a companion paper to ours that MO removal and early removal of paternal mitochondria occurs via distinct and separate ubiquitin-dependent process (Molina et al., 2019).

Autophagy is required for PME in *C. elegans*, with ATG8/LC3 ubiquitin-like proteins LGG-1 and LGG-2 being recruited around sperm mitochondria (Sato and Sato, 2011; Zhou et al., 2011; Al Rawi et al., 2011). LGG-1 is required for autophagosome formation while LGG-2 participates in microtubule-dependent transport toward the pericentrosomal area prior to acidification (Djeddi et al., 2015). Given that mammalian FUNDC1 binds directly to LC3, we reasoned that recruitment of these factors to paternal mitochondria may be impacted by *fndc-1(lf)*. However, both endogenous LGG-1 and LGG-2 (expressed maternally) appeared to localize normally around sperm mitochondria in 2-cell embryos following fertilization by *fndc-1(lf)* mutant males (Fig. 4B). We hypothesize that this result reflects functional redundancy in LGG recruitment, perhaps through other ubiquitin-independent mitophagy receptors.

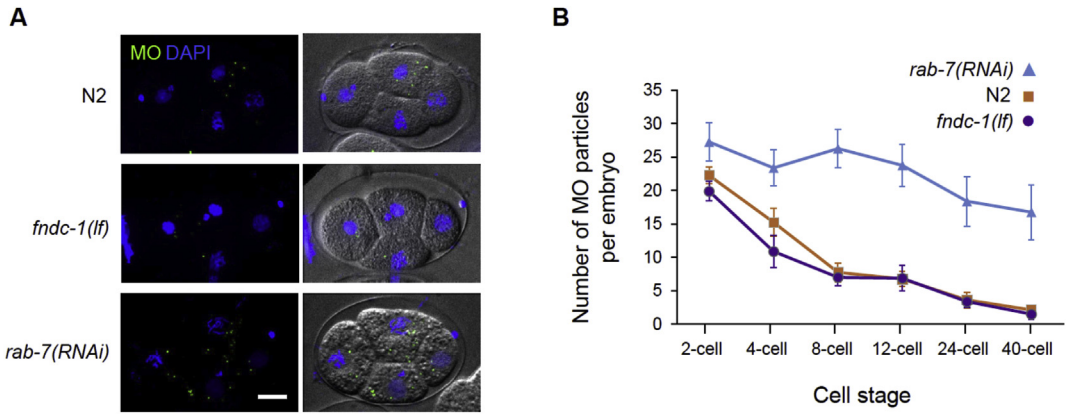

Fig. 3. Membranous organelles are effectively cleared in the absence of paternal FNDC-1. (A) No defect in MOs elimination is observed in the absence of FNDC-1 compared to wildtype (N2) embryos. A delay in MOs elimination can be observed in the *rab-7(RNAi)* embryos. Maximum-intensity Z-stacks projections of fixed embryos. Wildtype (N2), *fndc-1(lf)* and *rab-7(RNAi)* 4-cell stage embryos labeled for MOs (green) and stained for DNA (blue) (left panels) and DIC images (right panels) are shown. Scale bar: 10 μm. (B) Quantification of MO particles per cell stage in wildtype (N2) (purple), *fndc-1(lf)* (orange) and *rab-7(RNAi)* (blue) embryos (n = 8 embryos per condition). Data shown in the graph corresponds to the mean ± SEM of MOs per embryo.

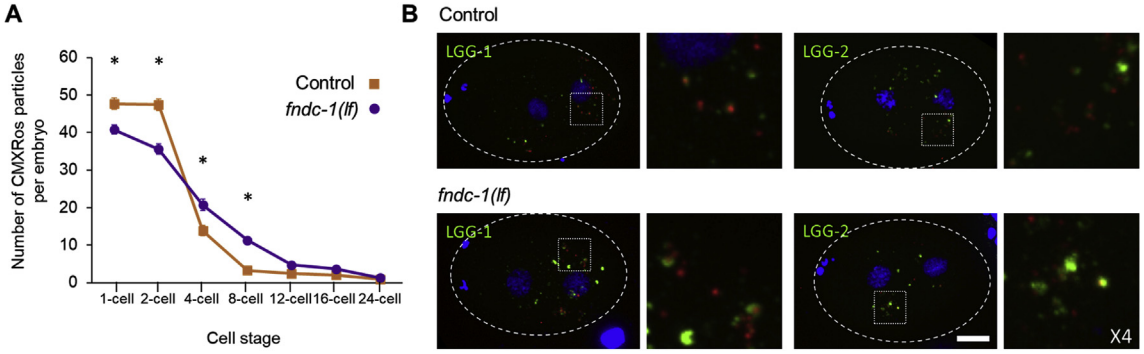

Fig. 4. Paternal FNDC-1 facilitates mitophagy at fertilization. (A) Quantification of CMXRos stained sperm mitochondria per cell stage in embryos from control (orange) and *fndc-1(lf)* (purple) male matings (n = 5 separate experiments with n ≥ 15 embryos analyzed for each stage). Data shown in the graph corresponds to the mean ± SEM of CMXRos particles per embryo. *p < 0.05; *t*-test (p-values: 1-cell, 8.8E-04; 2-cell, 1.6E-06; 4-cell, 1.9E-03; 8-cell, 1.2E-09). (B) Recruitment of autophagosome markers, LGG-1 and LGG-2, around sperm-labeled mitochondria can be observed in the absence of FNDC-1. Maximum-intensity Z-stacks projections of cross-fertilized 2-cell stage embryos from wildtype unlabeled hermaphrodites and either *fndc-1(lf)* or control CMXRos labeled males. Embryos are labeled for LGG-1 (green; top panels) and LGG-2 (green; bottom panels); CMXRos was used to label sperm mitochondria (red) and DAPI to visualize DNA (blue). For clarity, 4-fold magnifications of the highlighted areas are shown in the right panels. However, the entire embryo was analyzed to generate the quantitative data presented in panel A. Scale bar: 10 μm.

3. Discussion

The asymmetric expression of FNDC-1 on sperm mitochondria and the delayed PME in the *fndc-1(lf)* mutant suggest an attractive idea: that ubiquitin-independent mitophagy receptors may contribute to the selectivity filter that restricts mitochodrial degradation to the male germ line derived organelles. CPS-6, a mitochondrial endonuclease G, serves as the sole example of a paternal mitochondrial factor that is critical for PME (Zhou et al., 2016). Other molecules such as the core autophagy machinery that regulate PME appear to be contributed through the maternal germline (Ward and Gall, 1986) and are required for both MO clearance and mitophagy. In contrast, we have shown that FNDC-1 is contributed through the paternal germ line, is specific to PME, and has no role in the clearance of MO. Also, FNDC-1 is not required for recruitment of either LGG-1 or LGG-2 to sperm derived organelles. However, we have not ruled out a role for FNDC-1 in contributing to the stabilization of these proteins following their initial recruitment or that FNDC-1 may act at a later step in autophagosome formation. Of course, FNDC-1 could also act redundantly with other ubiquitin independent mitophagy receptors. To distinguish between these possibilities, it may be necessary to develop reagents that are better able to probe the discreet steps involved in PME downstream of ATG-8/LC3 protein recruitment.

We note that there is an apparent discrepancy between the persistence of *uaDf5* mtDNA in *fndc-1(lf)* mutant L1 larva (Fig. 2) versus the "delay" observed in PME as assessed by CMXRos labeled sperm mitochondria (Fig. 4). It is known that CMXRos staining disappears more quickly than genomic material, with published data showing that *uaDf5* can be detected up to the 64-cell stage in WT worms, even though CMXRos is entirely gone well prior to that (Zhou et al., 2011). This could illustrate the sensitivity of PCR over conventional fluorescent imaging approaches, although it is also possible that mitochondrial fusion/fission events could enable mtDNA from the sperm to be transferred to a maternal mitochondria. It is important that this effect appears to be exacerbated in the *fndc-1(lf)* mutant.

In this study, we have shown that the FNDC-1 is strongly expressed in the male germ line and contributes to PME assurance. However, we have not interrogated the mechanisms coordinating FNDC-1 activity with fertilization. In somatic cells, FUNDC1 helps coordinate the signaling pathway mediating mitochondrial fission and fusion by interacting with MARCH5, OPA1, calnexin, and DRP1 at the mitochondrion-associated membrane (Wu et al., 2017b), and mitochondrial dynamics are important for PME (Wang et al., 2016). Whether the same signaling pathways and interactions that have been defined in mammals act in a similar fashion in worms and can be applied to fertilization remains to be

determined.

It is notable however that calcium signaling at fertilization is well-established in both worms and mammals (Samuel et al., 2001; Miao and Williams, 2012) and that calcium-induced reactive oxygen species (ROS) produced at fertilization have recently been shown to control the early embryonic cell cycle in *Xenopus* (Han et al., 2018). Hence, it would not be difficult to envision an elegant process involving hypoxic stimulation of ROS generation to link the somatic and germ cell functions of FNDC-1.

In summary, our results demonstrating paternal germline expression of FNDC-1 and its role in PME should motivate further examination of ubiquitin-independent mitophagy receptors in the early embryo.

4. Materials and methods

4.1. C. elegans strains and maintenance

Strains were maintained under standard conditions at 20 °C on the *E. coli* OP50 seeded NGM plates. The bacterial clone for *rab-7* RNAi came from the J. Ahringer library and empty vector L4440 was used for control RNAi feeding experiments (Samuel et al., 2001).

Strains used in this study were the parental N2 Bristol strain and the following:

APW202 *ucr-2.3(jbm39 [ucr-2.3::gfp])*III.
CB3844 *fem-3(e2006)*IV.
CU607 smIs23[*pdk-2:gfp*]II; *him-5(e1490)*V.
KWN638 *fndc-1(rny15 [mRuby3:;fndc-1])*II.
KWN703 *fndc-1(rny14)*II.
KWN706 *fndc-1(rny14)*II; *him-5(e1490)*V; *uaDf5/+*
KWN708; *him-5(e1490)*V; *uaDf5/+*
KWN722 *fndc-1(rny15 [mRuby3:;fndc-1])*II; *him-5(e1490)*V.
KWN774 *ucr-2.3(jbm39)*; *fndc-1(rny15 [mRuby3:;fndc-1])*II.
KWN775 *fndc-1(rny14)*; *him-5(e1490)*V.

4.2. Generation of the fndc-1 transgenic worms

The *fndc-1* deletion and transgenic worm lines were generated via CRISPR-Cas9-triggered homologous recombination following a previously described method (Paix et al., 2017). The crRNAs were obtained from Dharmacon, Inc. (Lafayette, CO), and 6xHis-Cas9 was purified by conventional nickel column chromatography. A crRNA containing a guide sequence near a *Cla*I site in the first exon of *fndc-1* (GUAGUAGAGGACUGUAUCGATGG) (the adjacent protospacer motif (PAM) is underlined, but is not present in the crRNA) was injected with purified Cas9 enzyme and *dpy-10* crRNA as a co-injection marker. The deletion mutant was identified by single worm genomic PCR of *dpy-10* rol mutants using primers flanking the targeting site and screening of the PCR product by *Cla*I digest, as the *Cla*I site was disrupted by non-homologous end joining during the repair process. The *rny15* allele was created through homology-directed repair (HDR) using a crRNA guide sequence where the PAM was within the *fndc-1* start codon (CUGUGAUUGUUCCAGCCATGG) and a PCR repair template containing the mRuby3 coding sequence with 35 nt arms homologous to the genome on either side of the cleavage site that disrupted the PAM. All CRISPR-Cas9 generated clones were fully sequenced within several hundred nucleotides of the modification site and outcrossed to the ancestral N2 strain prior to use.

4.3. Detection of uaDf5 mtDNA

To assess *uaDf5* and wildtype mtDNA abundance in adult worms, lysis and PCR was performed as described (Gitschlag et al., 2016). Lysis was performed for 60 min at 65 °C in 10–30 µl of lysis buffer (50 mM KCl, 10 mM Tris, 20 mM MgCl2, 0.45% NP40, 0.45% Tween-20, 0.01% gelatin) containing 1 mg/ml proteinase K, followed by 15 min of inactivation at 95 °C. PCR was performed using three primers in combination: a mutant-specific forward primer 5′-CCATCCGTGCTAGAAGACAA-3′ with the wildtype-specific forward primer 5′-TTGGTGTTACAGGGGCAACA-3’ (in the region spanning the deletion), and reverse primer 5′-CTTCTACAGTGCATTGACCTAGTC-3′ common to both mutant and wildtype mtDNA. PCR products were separated on a 2% agarose gel, stained with ethidium bromide, and photographed under UV illumination. Band intensities were measured using Image Lab software (BioRad). To quantify PME efficiency, the relative abundances of wildtype and *uaDf5* mtDNA were measured in cross-progeny. 30–40 young adult males heteroplasmic for *uaDf5* were mated with 12 feminized *fem-3(e2006)* L4 stage worms at 20 °C for 16 h. After mating, gravid females were transferred to new NGM plate to obtain eggs for 3 h. The females were removed from the plates, which were then incubated at 20 °C overnight. The next day, 100 L1 progeny were harvested from each of the plates, lysed and analyzed as described above, with the following modification: separate PCR reactions were used to detect the wildtype and *uaDf5* mtDNA with the appropriate primer pairs. This was necessary due to the low abundcance of *uaDf5* in the L1 cross-progeny. Two experimental replicates each consisting of three sets of independent matings were performed on different days.

4.4. MitoTracker CMXRos staining to monitor PME

To stain mitochondria in male sperm, L4 stage male worms were transferred to NGM plates containing Mitotracker Red CMXRos (1 µg/ml, Molecular Probes) for 12 h in the dark. Prior to microscopy, the worms were placed onto new unlabeled NGM plates for 1 h. Sperm were isolated from male worms according to a previously reported protocol (Singaravelu et al., 2011). To monitor PME, labeled males were crossed with wildtype unlabeled young adult hermaphrodites overnight at 15 °C. Hermaphrodites with labeled spermatheca, indicating cross-fertilization, were picked under a fluorescence binocular dissecting microscope.

4.5. Fixation of embryos

Hermaphrodites were dissected directly on poly-l-lysine–coated glass slides. Embryo eggshells were opened by freeze cracking and immediately fixed in pre-cooled methanol for 20 min at −20 °C. Slides were rehydrated in phosphate-buffered saline (PBS) with 0.1% Tween 20 and blocked with 5% milk PBS-T. Embryos were incubated with primary antibodies for 2 h at room temperature and then washed two times for 30 min in PBS with 0.1% Tween 20. Secondary antibodies’ incubation was done for 1 h at room temperature. The embryos were washed as before and mounted with VECTASHIELD® Antifade Mounting Medium with DAPI (Vector Laboratories).

4.6. Antibodies

An affinity-purified rabbit polyclonal antibody against LGG-1 (Al Rawi et al., 2011), a mouse monoclonal antibody against peptides VPSFKERRPFHERQ and NSMSMSNLYSQERD of LGG-2, and the SP56 monoclonal antibody (generous gift from S. Strome (Ward and Gall, 1986)) were used to immunolocalize LGG-1 (1:200), LGG-2 (1:25) and MO (1:25) respectively in fixed embryos. Fluorescent secondary antibodies (1:500) were from Invitrogen and included anti-mouse Alexa-488, anti-rabbit Alexa 568 and anti-rabbit Alexa 488.

4.7. Fluorescent imaging

Paralyzed (with 0.1% tetramisole) worms or isolated sperm were mounted on 2% agarose pads on glass slides for microscopic examination using an Olympus FV1000 confocal microscope and FV10-ASW version 4 software (University of Rochester Light Microscopy Core). For the quantification of the number MOs and sperm mitochondria in fixed embryos, all embryos were imaged as multi-channel stacks of images every 0.4 µm (close to theoretical 0.29 optimal resolution) on a Zeiss Cell

Observer spinning disk microscope and maximum intensity projection were generated using ImageJ and Zen 2012 (blue edition) in order to count the number of particles. Embryonic stages were established by counting the number of DAPI labeled nuclei.

4.8. Statistical analyses

Since most of our datasets satisfied the conditions of normality, equal variance, and independence, two-sample unpaired t-tests were used to assess significance between genotypes.

Acknowledgements

Strains were provided by the *Caenorhabditis* Genetic Center and by Dr. Andrew Wojtovich whom we thank in particular for the *ucr-2.3*::GFP strain. Technical assistance provided by Teresa Sherman was greatly appreciated. This work was supported by R01 HL127891 (KN, PSB, YI, PS), NIH R15 HD083882 (PM), the Fondation pour la Recherche Médicale (Equipe FRM DEQ20160334874) and the European COST Program (BM1408 GENiE) (VG and KR).

References

Al Rawi, S., Louvet-Vallée, S., Djeddi, A., Sachse, M., Culetto, E., Hajjar, C., Boyd, L., Legouis, R., Galy, V., 2011. Postfertilization autophagy of sperm organelles prevents paternal mitochondrial DNA transmission. Science 334, 1144–1147.

Djeddi, A., Al Rawi, S., Deuve, J.L., Perrois, C., Liu, Y.-Y., Russeau, M., Sachse, M., Galy, V., 2015. Sperm-inherited organelle clearance in *C. elegans* relies on LC3-dependent autophagosome targeting to the pericentrosomal area. Development 142, 1705–1716.

Gitschlag, B.L., Kirby, C.S., Samuels, D.C., Gangula, R.D., Mallal, S.A., Patel, M.R., 2016. Homeostatic responses regulate selfish mitochondrial genome dynamics in *C. elegans*. Cell Metabol. 24, 91–103.

Hajjar, C., Sampuda, K.M., Boyd, L., 2014. Dual roles for ubiquitination in the processing of sperm organelles after fertilization. BMC Dev. Biol. 14, 6.

Han, Y., Ishibashi, S., Iglesias-Gonzalez, J., Chen, Y., Love, N.R., Amaya, E., 2018. Ca^{2+}-induced mitochondrial ROS regulate the early embryonic cell cycle. Cell Rep. 22, 218–231.

Lin, Y.-F., Schulz, A.M., Pellegrino, M.W., Lu, Y., Shaham, S., Haynes, C.M., 2016. Maintenance and propagation of a deleterious mitochondrial genome by the mitochondrial unfolded protein response. Nature 533, 416–419.

Liu, L., Feng, D., Chen, G., Chen, M., Zheng, Q., Song, P., Ma, Q., Zhu, C., Wang, R., Qi, W., et al., 2012. Mitochondrial outer-membrane protein FUNDC1 mediates hypoxia-induced mitophagy in mammalian cells. Nat. Cell Biol. 14, 177–185.

Miao, Y.-L., Williams, C.J., 2012. Calcium signaling in mammalian egg activation and embryo development: the influence of subcellular localization. Mol. Reprod. Dev. 79, 742–756.

Molina, P., Lim, Y., Boyd, L., 2019. Ubiquitination is required for the initial removal of paternal organelles in C. elegans. Dev Biol. https://doi.org/10.1016/j.ydbio.2019.05.015 pii: S0012–1606(19)30067-3. [Epub ahead of print] PMID: 31153831.

Paix, A., Folkmann, A., Seydoux, G., 2017. Precision genome editing using CRISPR-Cas9 and linear repair templates in *C. elegans*. Methods 121–122, 86–93.

Rawi, S Al, Louvet-Valle, Djeddi, A., Sachese, M., CUletto, E., Hajar, C., Boyd, L., Legouis, R., Galy, V., 2011. Postfertilization autophagy of sperm. Science 334 (80-), 1144–1147.

Rojansky, R., Cha, M.-Y., Chan, D.C., 2016. Elimination of paternal mitochondria in mouse embryos occurs through autophagic degradation dependent on PARKIN and MUL1. Elife 5.

Samuel, A.D.T., Murthy, V.N., Hengartner, M.O., 2001. Calcium dynamics during fertilization in *C. elegans*. BMC Dev. Biol. 1, 1–6.

Sato, M., Sato, K., 2011. Degradation of paternal mitochondria by fertilization-triggered autophagy in *C. elegans* embryos. Science 334, 1141–1144.

Sato, M., Sato, K., Tomura, K., Kosako, H., Sato, K., 2018. The autophagy receptor ALLO-1 and the IKKE-1 kinase control clearance of paternal mitochondria in *Caenorhabditis elegans*. Nat. Cell Biol. 20, 81–91.

Shakes, D.C., Ward, S., 1989. Mutations that disrupt the morphogenesis and localization of a sperm-specific organelle in *Caenorhabditis elegans*. Dev. Biol. 134, 307–316.

Singaravelu, G., Chatterjee, I., Marcello, M.R., Singson, A., 2011 Jan 31. Isolation and in vitro activation of *Caenorhabditis elegans* sperm. J. Vis. Exp. (47) https://doi.org/10.3791/2336 pii: 2336.

Tsang, W.Y., Lemire, B.D., 2002. Stable heteroplasmy but differential inheritance of a large mitochondrial DNA deletion in nematodes. Biochem. Cell Biol. 80, 645–654.

Wang, Y., Zhang, Y., Chen, L., Liang, Q., Yin, X.-M.M., Miao, L., Kang, B.-H.H., Xue, D., 2016. Kinetics and specificity of paternal mitochondrial elimination in *Caenorhabditis elegans*. Nat. Commun. 7, 12569.

Ward, S., 1986. The asymmetric localization of gene products during the development of *Caenorhabditis elegans* spermatozoa. In: Gall, J. (Ed.), Gametogenesis and the Early Embryo, vols. 55–75. A.R. Liss, New York, pp. 55–75.

Wei, Y., Chiang, W.-C., Sumpter, R., Mishra, P., Levine, B., 2017. Prohibitin 2 is an inner mitochondrial membrane mitophagy receptor. Cell 168, 224–238 e10.

Whitworth, A.J., Pallanck, L.J., 2017. PINK1/Parkin mitophagy and neurodegeneration-what do we really know in vivo? Curr. Opin. Genet. Dev. 44, 47–53.

Wu, H., Xue, D., Chen, G., Han, Z., Huang, L., Zhu, C., Wang, X., Jin, H., Wang, J., Zhu, Y., et al., 2014. The BCL2L1 and PGAM5 axis defines hypoxia-induced receptor-mediated mitophagy. Autophagy 10, 1712–1725.

Wu, W., Tian, W., Hu, Z., Chen, G., Huang, L., Li, W., Zhang, X., Xue, P., Zhou, C., Liu, L., et al., 2014. ULK1 translocates to mitochondria and phosphorylates FUNDC1 to regulate mitophagy. EMBO Rep. 15, 566–575.

Wu, W., Lin, C., Wu, K., Jiang, L., Wang, X., Li, W., Zhuang, H., Zhang, X., Chen, H., Li, S., et al., 2016. FUNDC1 regulates mitochondrial dynamics at the ER-mitochondrial contact site under hypoxic conditions. EMBO J. 35, 1368–1384.

Wu, S., Lu, Q., Wang, Q., Ding, Y., Ma, Z., Mao, X., Huang, K., Xie, Z., Zou, M.-H.H., 2017. Binding of FUN14 domain containing 1 with inositol 1,4,5-trisphosphate receptor in mitochondria-associated endoplasmic reticulum membranes maintains mitochondrial dynamics and function in hearts in vivo. Circulation 136, 2248–2266.

Wu, X., Wu, F.-H., Wu, Q., Zhang, S., Chen, S., Sima, M., 2017. Phylogenetic and molecular evolutionary analysis of mitophagy receptors under hypoxic conditions. Front. Physiol. 8, 539.

Yoo, S.-M., Jung, Y.-K., 2018. A molecular approach to mitophagy and mitochondrial dynamics. Mol. Cells 41, 18–26.

Zhang, W., Ren, H., Xu, C., Zhu, C., Wu, H., Liu, D., Wang, J., Liu, L., Li, W., Ma, Q.Q., et al., 2016. Hypoxic mitophagy regulates mitochondrial quality and platelet activation and determines severity of I/R heart injury. Elife 5, 71–86.

Zhou, Q., Li, H., Xue, D., 2011. Elimination of paternal mitochondria through the lysosomal degradation pathway in *C. elegans*. Cell Res. 21, 1662–1669.

Zhou, Q., Li, H., Li, H., Nakagawa, A., Lin, J.L.J., Lee, E.-S., Harry, B.L., Skeen-Gaar, R.R., Suehiro, Y., William, D., et al., 2016. Mitochondrial endonuclease G mediates breakdown of paternal mitochondria upon fertilization. Science 353, 394–399.